AGU PUBLICATIONS

JGR

Journal of Geophysical Research: Solid Earth

RESEARCH ARTICLE
10.1002/2017JB014578

Key Points:
- We locate ambient noise sources in glaciers by backprojecting cross-correlation time series
- Two major moulins were located, and both have diurnal activity related to melting in the daytime
- The correlation between precipitation and seismic activity is significant at timescales longer than a day

Supporting Information:
- Supporting Information S1
- Data Set S1
- Data Set S2
- Data Set S3
- Data Set S4
- Data Set S5
- Data Set S6

Correspondence to:
N. Aso,
aso@eps.s.u-tokyo.ac.jp

Citation:
Aso, N., Tsai, V. C., Schoof, C., Flowers, G. E., Whiteford, A., & Rada, C. (2017). Seismologically observed spatiotemporal drainage activity at moulins. *Journal of Geophysical Research: Solid Earth*, *122*, 9095–9108. https://doi.org/10.1002/2017JB014578

Received 17 JUN 2017
Accepted 17 OCT 2017
Accepted article online 19 OCT 2017
Published online 11 NOV 2017

Seismologically Observed Spatiotemporal Drainage Activity at Moulins

Naofumi Aso[1,2], Victor C. Tsai[1], Christian Schoof[3], Gwenn E. Flowers[4], Arran Whiteford[3], and Camilo Rada[3]

[1]Seismological Laboratory, California Institute of Technology, Pasadena, CA, USA, [2]Department of Earth and Planetary Science, University of Tokyo, Tokyo, Japan, [3]Department of Earth and Ocean Sciences, University of British Columbia, Vancouver, British Columbia, Canada, [4]Department of Earth Sciences, Simon Fraser University, Burnaby, British Columbia, Canada

Abstract Hydrology is important for glacier dynamics, but it is difficult to monitor the subsurface drainage systems of glaciers by direct observations. Since meltwater drainage generates seismic signals, passive seismic analysis has the potential to be used to monitor these processes. To study continuous seismic radiation from the drainage, we analyze geophone data from six stations deployed at the Kaskawulsh Glacier in Yukon, Canada, during the summer of 2014 using ambient noise cross-correlation techniques. We locate the noise sources by backprojecting the amplitude of the cross correlation to the glacier surface. Most of the ambient noise sequences are found in two clusters, with each cluster located in the vicinity of a moulin identified at the surface. Stronger seismic radiation is observed during the day, consistent with expected variability in melt rates. We demonstrate that the sparse seismic network array with 2 km station separation has the ability to detect moulins within the array with a precision of 50 m. We confirm that seismic activity is correlated with air temperature, and thus, melt, on a diurnal timescale, and precipitation correlates with the activity at longer timescales. Our results highlight the potential of passive seismic observations for monitoring water flow into subglacial channels through moulins with an affordable number of seismic stations, but quantification of water flow rates still remains a challenge. The cross-correlation backprojection technique described here can also potentially be applied to any localized source of ambient noise such as ocean noise, tectonic tremor, and volcanic tremor.

1. Introduction

Hydrology plays an important role in ice sheet and glacier dynamics in that meltwater can accelerate ice flow (e.g., Iken & Bindschadler, 1986) and contribute to the loss of ice. The effect of meltwater on ice flow manifests itself at a number of timescales, ranging from the seasonal scale of drainage system evolution (e.g., Zwally et al., 2002) to the weekly scale of synoptic weather patterns (e.g., van de Wal et al., 2008) and the diurnal scale of melt cycles (e.g., Davis et al., 2014) as well as even shorter timescales associated with rapid drainage events (e.g., Das et al., 2008). In addition, geological field surveys (e.g., Denis et al., 2010), laboratory experiments (e.g., Clarke, 2005), and numerical simulations (e.g., Schoof, 2010) suggest that increased meltwater can sometimes increase and sometimes decrease water pressure and therefore ice-flow rates. Such complex subglacial drainage behavior is traditionally thought to arise from one of two basic drainage configurations: a channelized system is thought to develop during the summer melt season as a result of increased water supply, enabling the growth of individual conduits through wall melting (Hock & Hooke, 1993; Röthlisberger, 1972), with a distributed system (or no drainage system at all) dominating at other times (Fountain & Walder, 1998). While the subglacial hydrological system is an important part of subglacial drainage, meltwater supply is also fundamentally important not only simply as an input of the system but also because it controls the evolution of the subglacial system (e.g., Andrews et al., 2014). In addition to seasonal changes, year-to-year evolution of the subglacial hydrological system and resultant change in dynamics are also controlled by meltwater supply (Doyle et al., 2014; Sundal et al., 2011). Thus, to understand subglacial drainage, which is determined by interactions between meltwater and the subglacial hydrological system, it is important to monitor both subglacial channel structure and meltwater supply.

Subglacial drainage has been traditionally investigated by borehole observations (e.g., Andrews et al., 2014; Hubbard et al., 1995) and dye tracer experiments (e.g., Burkimsher, 1983; Chandler et al., 2013). These direct in

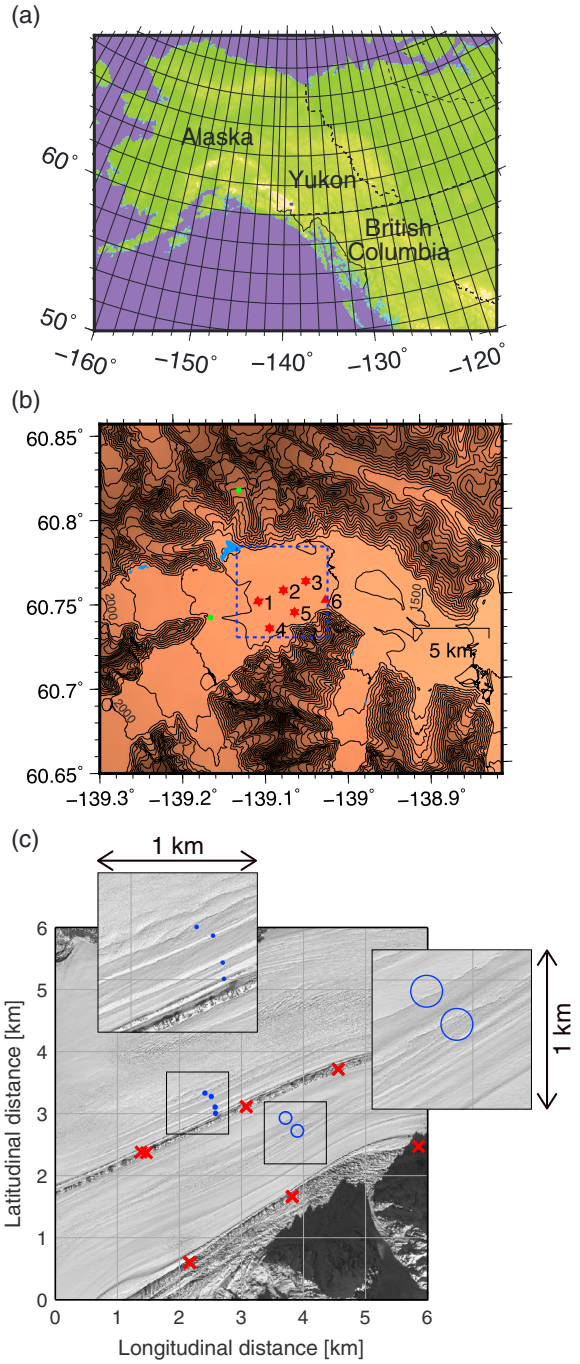

Figure 1. (a) Map of the study region. The small rectangle in the Yukon Territory is shown. (b) Station map with surface topography. The contour intervals are at 100 m spacing, and the stations are located at elevations of 1,600–1,700 m. The regular and inverted triangles represent the locations before and after the instrument replacement, respectively, which was done on 26 July 2014 (UTC-7). The green circles represent weather stations. The blue dashed line represents the area shown here and in Figures 4 and 5. (c) WorldView-1 image (panchromatic band on 4 October 2011, Polar Geospatial Center) of the study region. The origin point (bottom-left corner) of this map view is (602,000E, 6,734,000N) in UTM Zone 7. The red crosses represent station locations both before and after the instrument replacement. The blue dots and circles are the locations of moulins that were observed on site and from a helicopter, respectively, in the 2015 summer season. The insets show close-ups of the moulin locations.

situ observations can continuously monitor drainage but are spatially limited due to physical access to the bed at point locations. On the other hand, there are indirect observations from which hydrological inferences can be made including active seismic exploration (Kapitsa et al., 1996), airborne radio echo sounding (Oswald & de Q. Robin, 1973), and satellite altimetry (Ridley, Cudlip, & Laxon, 1993), which cover wider regions with lower spatial and temporal resolution. Passive seismic source analysis has the advantage of both being continuous and spatially distributed without requiring direct physical access and thus has the potential to observe subglacial drainage continuously at distant stations.

Recently, such passive seismic techniques have been used to study subglacial drainage. For example, Bartholomaus et al. (2015) observed seismic noise generated at a subglacial channel at Mendenhall Glacier in Alaska and Gimbert et al. (2016) estimated its channel geometry and discharge. In another application, microseismic tremor was observed to be generated at moulins at the Sermeq Avannarleq ablation zone near Jakobshavn Isbrae in Greenland (Röösli et al., 2014; Röösli et al., 2016; Walter et al., 2015). In addition to subglacial drainage, the passive seismic technique has also been used to study iceberg calving (Amundson et al., 2012) and icequakes (Carmichael et al., 2012, 2015; Walter et al., 2009) and is becoming a popular method to study a variety of different processes in glaciology. In this paper, we explore the use of passive seismic source analysis to monitor drainage.

For this purpose of studying seismic signals during drainage, we analyze geophone records from the Kaskawulsh Glacier in Yukon, Canada, during the summer of 2014, where a direct, visual determination of the main water supply routes to the subsurface would have been difficult. We develop a passive seismic analysis method to simultaneously determine the location and strength of multiple sources. Ultimately, we robustly identify two moulins that actively supply water to the glacier drainage system over a relatively large glacier surface area (~10 km^2) using only six stations.

2. Field Site and Instrumentation

Our study site is located near the confluence of the North and Central arms of the Kaskawulsh Glacier (approximately 605,000E, 6,737,000N in UTM Zone 7 and 1,650 m above sea level (asl); see Figure 1a; see Figure 3 of Waechter et al. (2015)). The field campaign was initially designed to study the drainage of a nearby ice-dammed lake (Johnson & Kasper, 1992) that slowly fills and rapidly drains every summer (Figure 1b). In this part of the Kaskawulsh Glacier, multiple supraglacial streams can be identified from the WorldView-1 satellite image (Figure 1c) of 4 October 2011, taken a few years before our observation period. There is some crevassing in particular areas in the middle of the north arm near (x,y) = (2 km,4 km) in Figure 1c, but the majority of the ice in the area is free of surface crevasses. Although we do not have a complete list of moulins, some moulins were also observed on site (both from the ground and air), and each of them was located within 50 m of the nearest supraglacial stream observed in the satellite image.

We deployed 10 single component geophone (FairfieldNodal ZLand) stations in total. Good signal coherency was observed only among six stations located on the south side of the Kaskawulsh Glacier, further from the ice-dammed lake than the remaining four stations. Note that the six coherent stations were located on the surface of the glacier itself, while the remaining four, which we exclude from the remainder of this study, were positioned on a well-compacted lateral moraine. The lower coherency of the moraine stations might be related to high attenuation in the moraine layer but is perhaps mainly because these stations are far from the major sources observed. We analyze geophone records from the six coherent stations from 15 July to 1 August 2014. All dates and times in this paper are given in local time (07:00 UTC). The instruments used for the study were replaced on 26 July, at which point station 6 was removed altogether because of difficulty in accessing the site. We focus on time periods with at least five stations available, from 15 July 19:00 to 26 July 11:00 before the replacement and from 26 July 23:00 to 1 August 8:00 after the replacement. The natural frequency of the geophones is 10 Hz, and the response curve falls off below 10 Hz, but the energy at 2–10 Hz remains observable, and this frequency band mainly contributes to this study's analyses. The recording sampling rate is 250 Hz, and the recorded seismogram is a vertical velocity seismogram, relative to the geophone stake. The geophones were placed in a vertical position with their stakes inserted into moraines on the glacier ice and the geophones covered by piles of larger rocks. The debris mantle on the glacier was invariably thin (less than 10 cm at all sites), and differential melting in all cases caused the rock piles on top of the geophones to shift. As a result, all geophones eventually toppled into a position with the stake oriented horizontally. We do not have any information on how quickly the toppling occurred and therefore do not know when the change from vertical component to horizontal component geophones occurred.

In addition to the seismic data, we also use meteorological data to compare with the results. Temperature data were collected at an automatic weather station at the confluence (1,845 m asl; ~5 km upstream, to the west of our study area), and precipitation data were collected with a tipping bucket ~5 km north of the study site (2,300 m asl). The co-located air temperature data were also used to estimate an effective lapse rate (−8.8°C/km from 1,845 m to 2,300 m asl). We estimate air temperature at the study site (1,650 m) by extrapolating the temperature record at the confluence using the lapse rate.

3. Cross-Correlation Backprojection

The low-amplitude seismic signal continuously radiated by water flow, either in subglacial channels (Winberry, Anandakrishnan, & Alley, 2009) or at moulins (Röösli et al., 2014), is difficult to recognize at a single station, but the signal can be captured by measuring the coherency between multiple stations. The seismic signals generated by a localized source and observed at two stations have a time shift that depends on the geometry of the source relative to the two stations. The time lag is observed as high coherency in the cross-correlation function between seismograms at two stations. Since multiple sources can produce several peaks in each cross correlation, we do not pick a single peak from the cross correlation but apply a backprojection technique (Ishii et al., 2005) to utilize all the information contained in the cross-correlation function. The general method is similar to that used by Heeszel, Walter, and Kilb (2014), but rather than backprojecting the raw data, here we backproject the cross-correlation data. This technique, which we call the cross-correlation backprojection method, was initially designed for electromagnetic imaging (Foo & Kashyap, 2004) and is now widely used in the Earth sciences. Its applications include the study of earthquake source processes (Meng et al., 2012), landslide evolution (Chao et al., 2015), and sediment transport in rivers (Burtin et al., 2010), as well as locating seismic scatterers (Ma et al., 2013) or microseismic sources in the ocean (Stehly, Campillo, & Shapiro, 2006) and locating moulins on glaciers (Walter et al., 2015). The backprojection process enables us to detect multiple simultaneous sources, and this is an advantage over conventional location methods that utilize a single peak in each cross-correlation function (Shapiro, Ritzwoller, & Bensen, 2006). We analyze cross correlations in the time domain, equivalent to analyzing cross-spectra in the frequency domain as done by Walter et al. (2015). Although Walter et al. (2015) applied singular value decomposition of the cross-spectral density matrix to distinguish different sources, we will show here that we can still identify multiple sources without such a decomposition.

While Walter et al. (2015) used the original record without preprocessing, we apply 1 bit normalization to enhance small but continuous signals and suppress spiky icequake signals as is often done in seismic

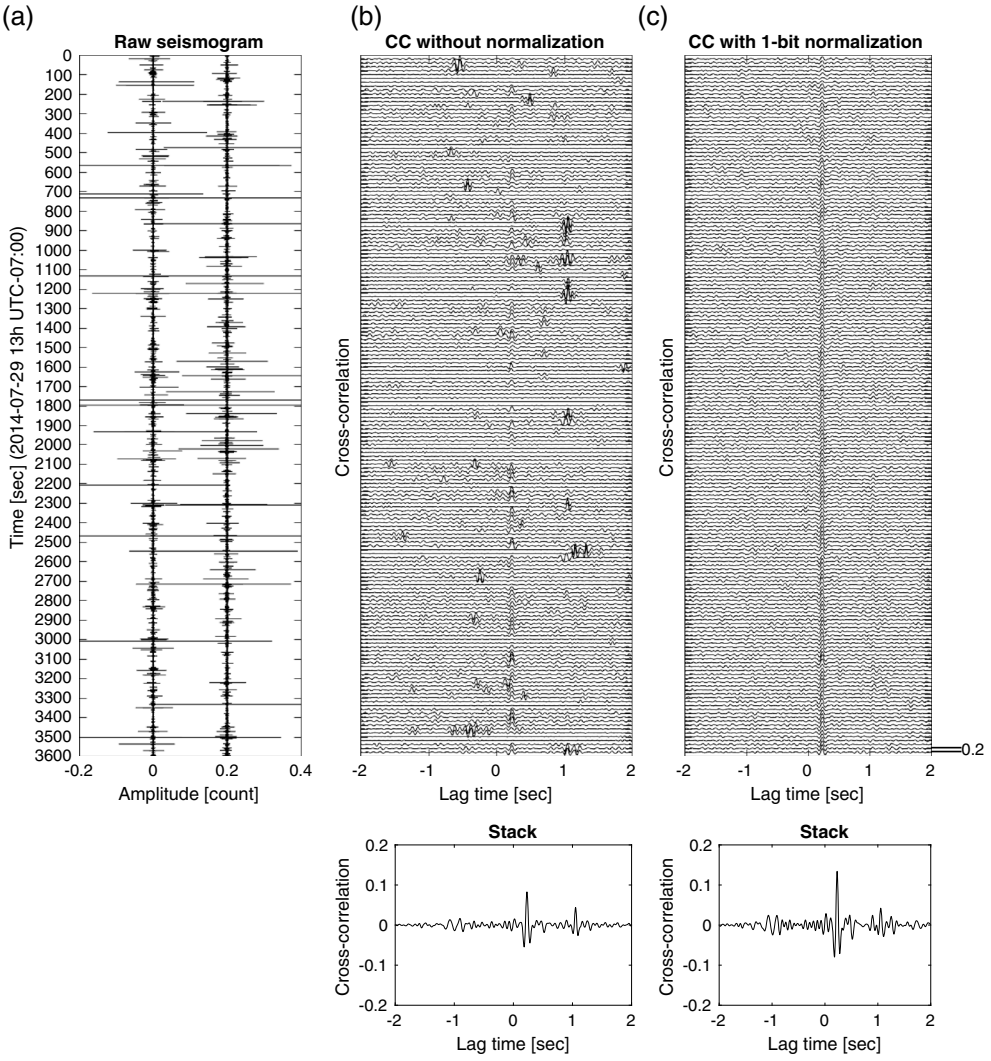

Figure 2. Demonstration of how 1 bit normalization works in cross correlation. (a) Original traces at stations 1 and 2 after band-pass filtering between 0.1 and 20 Hz. (b) Cross correlation of two traces in Figure 2a for half-overlapping 40 s windows. The cross correlation is band-pass filtered again. (c) Cross correlation with 1 bit normalization of two traces in Figure 2a for half-overlapping 40 s windows. The cross correlation is band-pass filtered again. (d) Stacked cross correlation for all time windows in Figure 2b. (e) Stacked cross correlation for all time windows in Figure 2c.

interferometry (e.g., Bensen et al., 2007). A comparison of cross correlation with and without 1 bit normalization is shown in Figure 2. To suppress small local icequakes, we also apply a low-pass filter at 20 Hz before and after computing the cross correlation. Although icequakes also radiate energy below 20 Hz, the obtained cross-correlation peaks are not consistent with arrival times of icequakes, and we conclude that icequakes do not influence the cross correlation significantly. We calculate the normalized cross correlation for each 40 s window with 20 s overlap and average them for each 1 h time period. In summary, we process data in the following order: 1 bit normalization, low-pass filtering, cross correlation, average stacking, and low-pass filtering again. The original data are not corrected for instrumental response because it has little effect on cross correlation, especially after the normalization process.

After the processing described above, we obtain the normalized cross-correlation $C_{ij}(\Delta t)$ between stations i and j as a function of lag time Δt for each hour, which takes values between -1 and 1 (Figure 3 shows examples for three different station pairs and three different time periods). In the present study, we define positive lag time as the time at station i relative to station j. A peak at a negative lag time represents a

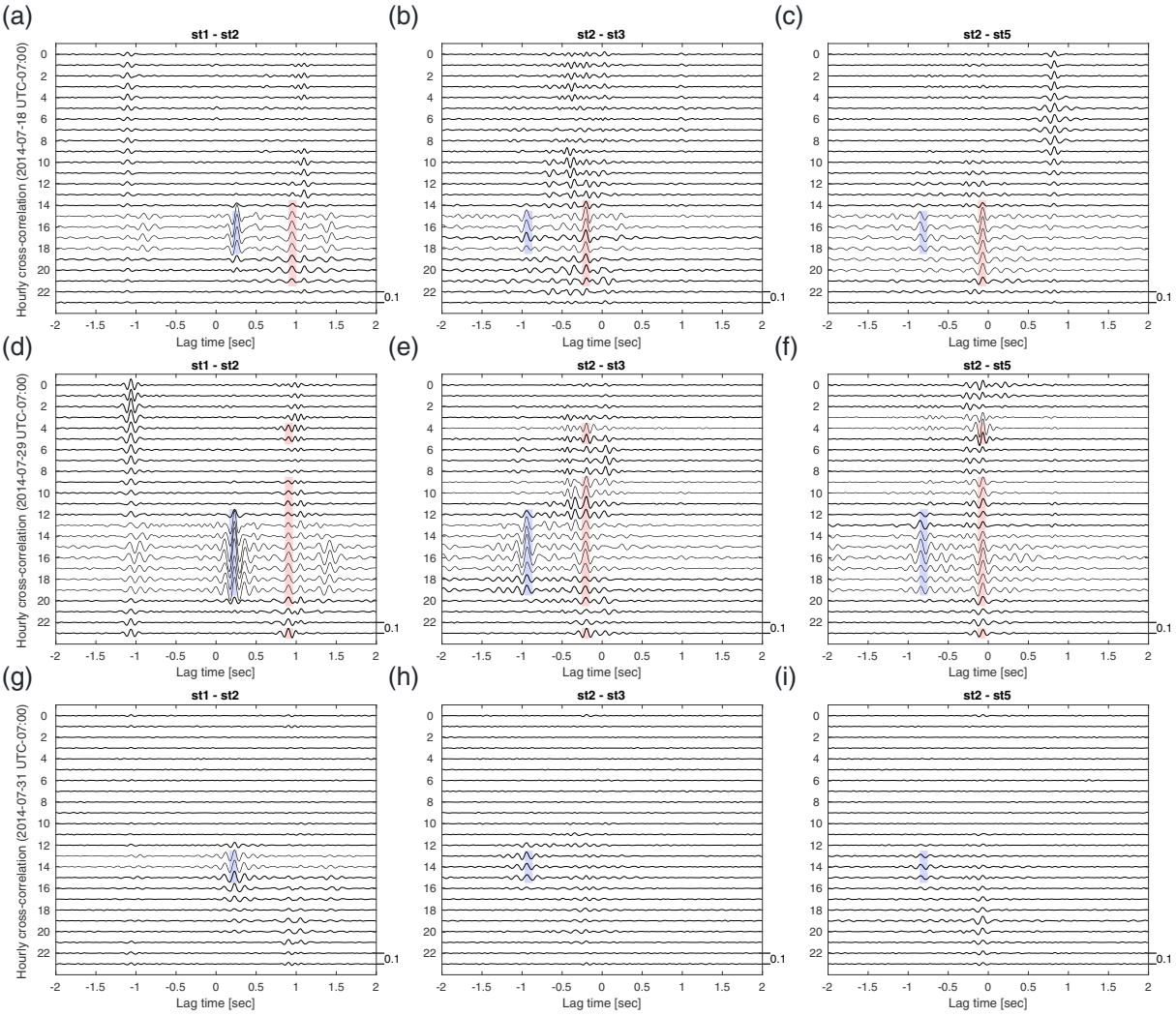

Figure 3. Temporal variation of cross correlation for each day. Each cross-correlation trace is calculated for a 1 h record. The blue and red stripes indicate differential arrival times expected for obtained locations of moulins A and B, respectively. (a) Between stations 1 and 2 on 18 July. (b) Between stations 2 and 3 on 18 July. (c) Between stations 2 and 5 on 18 July. (d) Between stations 1 and 2 on 29 July. (e) Between stations 2 and 3 on 29 July. (f) Between stations 2 and 5 on 29 July. (g) Between stations 1 and 2 on 31 July. (h) Between stations 2 and 3 on 31 July. (i) Between stations 2 and 5 on 31 July.

source closer to station *i* than *j*, opposite the convention in seismic interferometry but more intuitive regarding which station is closer to the localized source. We then take its envelope $E_{ij}(\Delta t)$ as

$$E_{ij}(\Delta t) = \left| C_{ij}(\Delta t) + i\mathcal{H}\left[C_{ij}(\Delta t)\right] \right|, \tag{1}$$

where $\mathcal{H}(u)$ represents the Hilbert transform of u. Finally, we apply backprojection and obtain the mean cross-correlation $A(\mathbb{x})$ at a spatial point $\mathbb{x}$ by taking an average of the cross-correlation envelope at the expected lag time as

$$A(\mathbb{x}) = \frac{2}{n(n-1)} \sum_{i=1}^{n-1} \sum_{j=i+1}^{n} E_{ij}\left(\tau_i(\mathbb{x}) - \tau_j(\mathbb{x})\right), \tag{2}$$

where $\tau_i(\mathbb{x})$ is the travel time from source $\mathbb{x}$ to station i and n is the number of stations. Here we assume that we are observing Rayleigh waves radiated from near-surface sources, and we calculate the backprojected amplitude on the ice surface. We have confirmed that the sources are located at the surface by locating the source depth assuming three-dimensional *S* wave propagation instead of two-dimensional Rayleigh

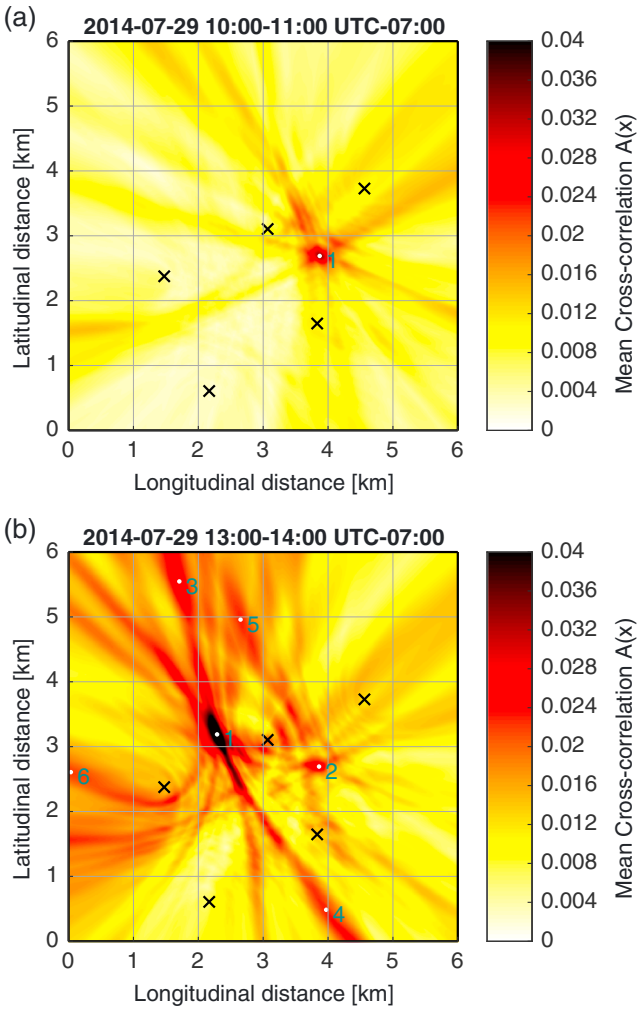

Figure 4. Example of cross-correlation backprojection at (a) 10:00–11:00 and (b) 13:00–14:00 on 29 July 2014. The origin (bottom-left corner) of this map is (602,000E, 6,734,000N) in UTM Zone 7. The colors represent backprojected cross-correlation amplitude, which is equivalent to an average cross-correlation value. Local maxima greater than the threshold 0.02 are shown by the white dots with numbers ordered by the peak value. We use only the first two peaks to avoid artifacts. Stations are shown with black crosses.

wave propagation. This test can robustly estimate source depth because surface sources are located on the surface even in the case where Rayleigh waves are misidentified as S waves, as long as we use differential arrival times. Synthetic calculations verify that the source is near the surface (depth < 100 m), so that Rayleigh waves are much stronger than body waves at the epicentral distances and frequencies of our study. We assume a Rayleigh wave velocity of 1.68 km/s for the travel time calculation, which is the theoretical value for a homogeneous half-space of ice, with a *P* wave velocity of 3.6 km/s and an S wave velocity of 1.8 km/s. Accurate velocity estimates are not available in the study region, and ice velocity is known to vary between glaciers (Rial, Tang, & Steffen, 2009; Röthlisberger, 1972), but we have verified that the results are similar for all assumed Rayleigh wave velocities in the range of 1.50–1.80 km/s.

We identify peaks of $A(x) \geq 0.02$ from the backprojected image (Figure 4) and select representative peaks by declustering so that all the peaks are separated by at least 1 km from each other. Since the third peak within each hourly image might be artificial due to interference between the first and second sources, we further analyze only the two largest peaks in each hourly image. The grid size of the backprojection is 2 m × 2 m, and the entire search region for peaks is a 6 km × 6 km square whose sides are aligned north-south and east-west, with Northing 602,000–608,000 and Easting 6,734,000–6,740,000 in UTM Zone 7. Each hourly period in which there is a detection we call a "tremor episode," and up to two tremor episodes with different locations can be resolved at the same time.

4. Results

We find several localized sources including two major clusters (Figure 5a). One (A in Figures 5a and 5b) is on the northern side of the medial moraine, and the other (B in Figures 5a and 5c) is located between the medial moraine and the southern glacier margin. From the very concentrated distribution of locations obtained within each cluster, we consider uncertainties in the source locations within each cluster to be 50 m. Both of these two source clusters are located along supraglacial channels that are visible in satellite imagery. We also obtain several other minor sources on the ice surface in addition to the two major clusters. We nevertheless focus only on the two major clusters in the present study because the minor clusters are much less active than the major clusters and their station coverage is also worse.

A number of lines of evidence support the interpretation that the seismic noise sources are moulins. First, the signals are generated near the surface as confirmed above, so they are not associated with subglacial streams or basal slip. Second, the noise sources are not widely distributed along the supraglacial channels but are instead strongly localized. Third, on-site aerial and ground-based observations in 2015 also later confirmed that moulins were present within 300 m of the computed source locations (Figures 5b and 5c). Lastly, from the viewpoint of seismic excitation, the vertical water flow into moulins is expected to generate stronger seismic waves than the main supraglacial stream; the loss of potential energy in the water flow is much greater per unit length of flow where the water descends into the moulin than where it follows a nearly horizontal surface channel.

We focus on the temporal pattern of the seismic activity at moulins, which is expected to be highly correlated with moulin discharge, although there may be other factors controlling the seismic radiation. A diurnal pattern of activity was found in both clusters. As the high activity was observed during the day, we infer that

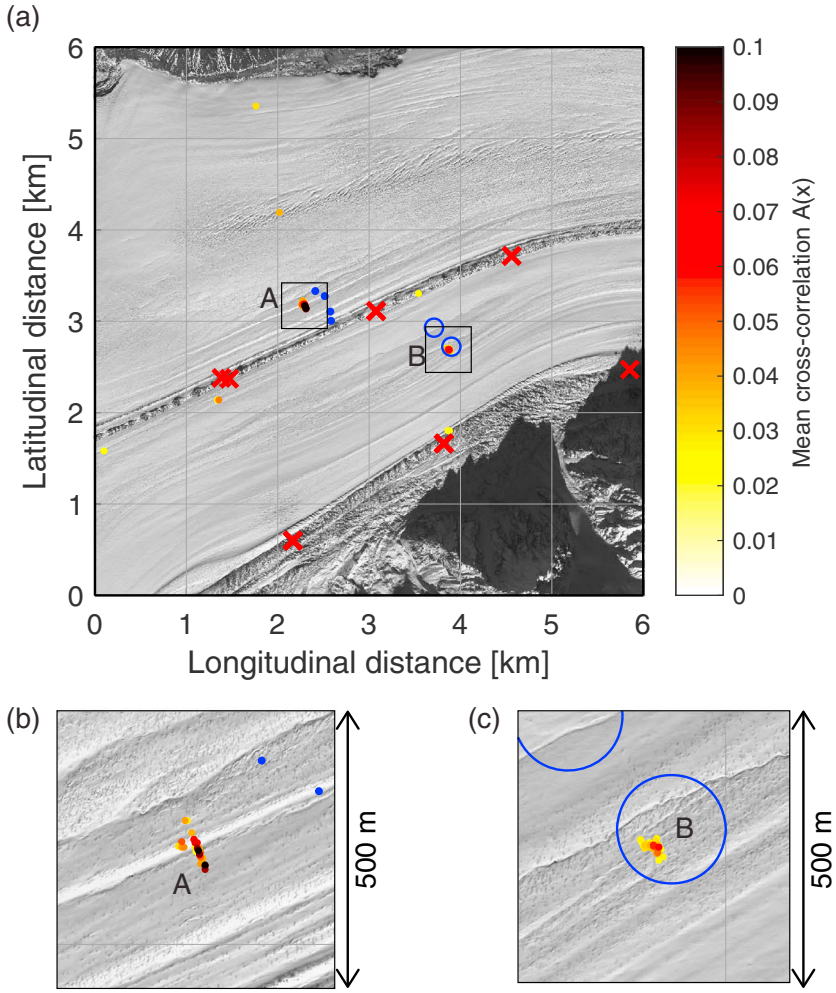

Figure 5. Noise source locations during the observation. (a) Noise source locations are shown with colored dots, with colors representing backprojected cross-correlation amplitudes. The origin point (bottom-left corner) of this map view is (602,000E, 6,734,000N) in UTM Zone 7. The blue dots and circles represent the moulins that were observed on the ground or from a helicopter, respectively, in the 2015 summer season. The red crosses represent station locations both before and after the instrument replacement. The black rectangles represent areas of close-ups in the next panels. (b) A close-up of moulin A. (c) A close-up of moulin B.

surface melting affects the seismic activity significantly, consistent with previous studies on the diurnal pattern of moulin discharge (e.g., McGrath et al., 2011). We observe 66 tremor episodes during the daytime (6:00–23:00), which is 25% of all of the daytime hours, and 6 episodes during the nighttime (0:00–5:00), which is 7% of all of the nighttime hours, in total. The concentrated occurrence during the daytime is expected with a probability of 1.3×10^{-4} (so-called *p*-value) assuming random distribution in time. We also observe the peak activity (i.e., the number of episodes) being slightly shifted from solar noon toward afternoon by 1–3 h. Considering that the highest temperatures are also observed 2–3 h after solar noon (Figure 6), our observation is consistent with no delay between peak temperature and peak water delivery to the moulins. This small delay is likely partially because the moulins drain meltwater that is produced locally and perhaps partially related to surface water flow speeds being relatively fast. However, since the activity of moulin B is slightly delayed from that of moulin A, moulin B might have a larger catchment area or a longer supraglacial stream feeding the moulin. Indeed, the central arm, where moulin B is located, has longer upstream tributaries, and the north arm, where moulin A is located, gains elevation more quickly.

Although the diurnal activity pattern indicates that temperature plays an important role in moulin activity, these moulins also radiate seismic signals during the night on colder days (Figure 6). When we examine

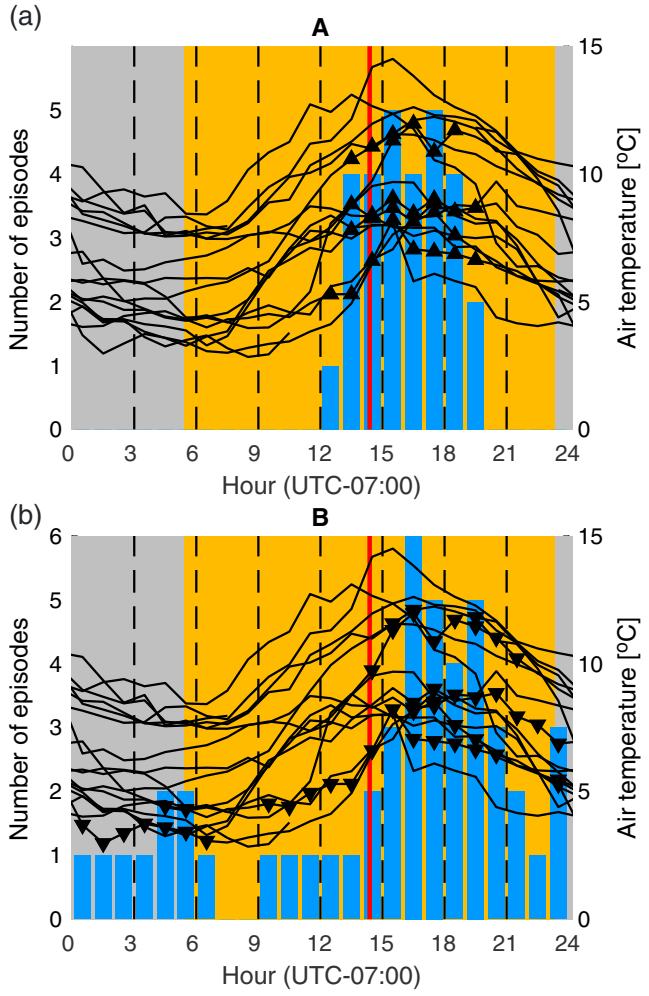

Figure 6. (a and b) Daily activity of the noise sources A and B are shown. Time is in UTC-7. The orange times represent daytime, and the gray times represent nighttime obtained from the National Oceanic and Atmospheric Administration (NOAA) website. The red vertical line represents the time of solar noon. The black lines are daily records of air temperature from an automatic weather station (1,845 m asl) located at the glacier confluence, a few kilometers west of the study region. The regular and inverted triangles represent detections at moulins A and B, respectively.

the seismic activity at timescales longer than a day (Figure 7a), we observe significant seismic activity on colder days in the later part of the observation period (Figure 7b). That activity on colder days is not consistent with glacier melt estimates using the positive degree-day method (e.g., Braithwaite, 1995) (Figure 7c), suggesting the existence of other important factors contributing to moulin activity. One possible factor besides temperature is precipitation, which is found to correlate positively with the observed activity at timescales longer than a day. To verify the correlation between precipitation and the moulin activity at timescales longer than a day, we compare the activity with daily precipitation (Figure 7d). We average 24 h of data starting from 21 h before the time of the moulin activity and ending 3 h afterward, because the precipitation record with a tipping bucket at the weather station at 2,300 m asl may be delayed due to snowmelt while only rain is expected at the study site during the observation period. For example, the small amounts of precipitation recorded from 29 July night to 30 July morning and a sharp peak on 30 July afternoon are thought to be associated with snowing at night and melting during the day at the weather station at 2,300 m asl, respectively. During periods with precipitation (54% probability corresponding to 209 h out of total 385 h), we observe 69% of the episodes (20 episodes out of 29) at moulin A and 79% of the episodes (38 episodes out of 48) at moulin B, which gives *p*-values of 0.036 and 8.8×10^{-5} for moulins A and B, respectively. It therefore appears that precipitation correlates moulin activity at timescales longer than a day, while temperature primarily controls the activity on a diurnal timescale. To further demonstrate the conditions necessary for seismic activity, in Figure 8, we plot both the detected tremor episodes and nondetections against temperature and precipitation. We could not find clear conditions for seismic activity, but it is notable that we observe seismic signals only when temperature was higher than the daily mean temperature or the daily mean precipitation was $\geq$1 mm/d. We also note that most of the positive detections during high precipitation and low temperature are for moulin B (red dots in Figure 8), suggesting that the two moulins may be affected differently by precipitation. Since rainfall is unlikely to have overtaken melt as a dominant water source over the entire glacier, other factors that relate to both melting and precipitation, and which may produce the apparent correlation, will be discussed later, though it is possible that precipitation may locally dominate meltwater in some locations (such as over moulin B's catchment).

Here we note that station coverage is different for our two main sources. The data quality also changes due to the replacement of geophones on 26 July, and it also gradually changes during the observation period due to temporally varying coupling between the geophones and ice. Hence, though some of the variability in activity observed in Figure 7 may be spurious, some temporal characteristics of the activity is still worth mentioning. During the first half of the observation period, precipitation of $<$1 mm/h exists, but the diurnal moulin activity does not seem to be altered (Figure 7d). The diurnal pattern at moulin A is also not affected even by substantial rainfall (~5 mm/h) during the second half of the observation period. Although it is not clear whether the activity completely shuts down or whether there exists weak flow at the moulin at night, there is no doubt that the activity is much weaker at night; the observed signal is clearer during the day even though stronger noise from other sources is also expected. On the other hand, the activity at source B on a diurnal timescale changes from periodic to nearly continuous on 29 July during precipitation (compare Figures 3a–3c for 18 July with Figures 3d–3f for 29 July). There still exists a diurnal modulation of activity, but the activity at night during this period is significant (Figures 3d–3f). This significant difference in how moulins A and B are affected by precipitation suggests that there may be significant heterogeneity of moulin response to precipitation and

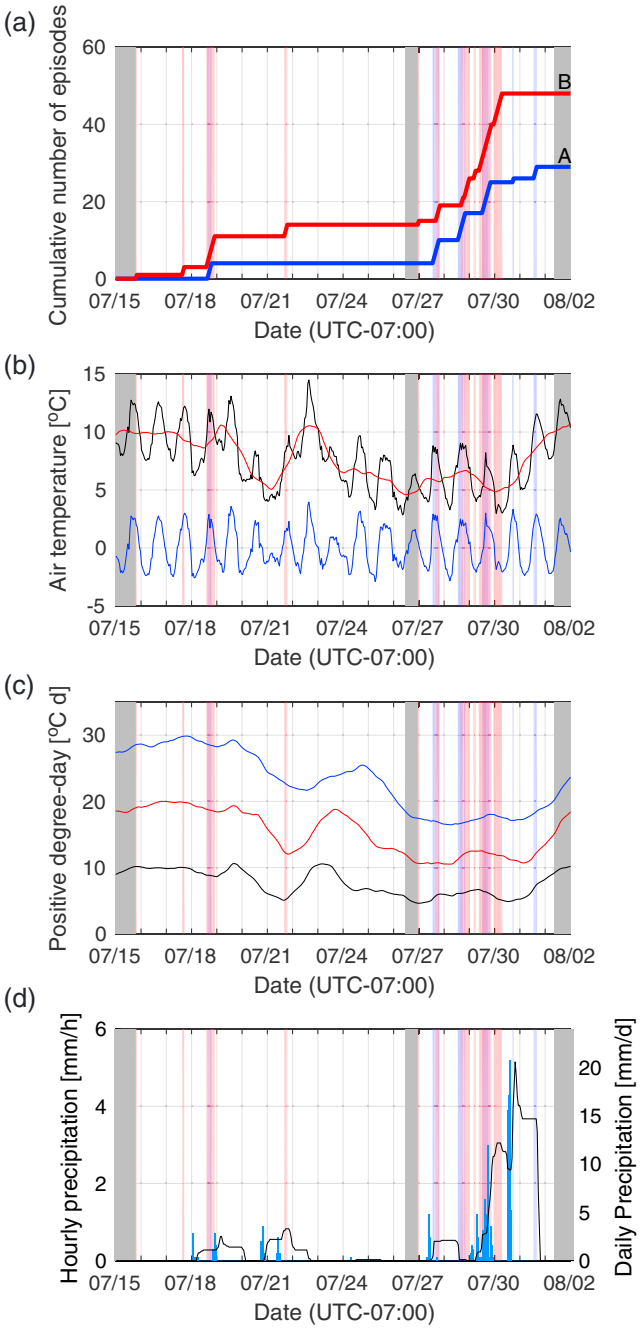

Figure 7. Seismic activity and relevant meteorological data during the observation period. The seismic activity at moulins A and B are marked by the background blue and red stripes in each panel, respectively. The gray stripes represent time periods we do not analyze due to an insufficient number of available stations. (a) Cumulative number of seismic episodes at moulins A and B are shown in blue and red lines, respectively. (b) The black line represents estimated air temperature at the study site. The red line is daily average temperature, and the blue line is temperature deviation (the difference between black and red). (c) Positive degree day estimates of melt at the study site estimated with time windows of 1 day (black), 2 days (red), and 3 days (blue). (d) The blue bars represent hourly precipitation recorded at an automatic weather station (2,300 m asl) on a small glacier located a few kilometers north of the study region. The black line represents daily precipitation calculated from 21 h before to 3 h later.

will be discussed further in the next section. A second interesting temporal change is that moulin A is significantly more active than moulin B from 31 July onward (see Figure 7a). In fact, moulin B is observed to be more active before the geophone replacement, and the activity of moulins A and B is comparable after the replacement (Figure 7a), but this is probably because data quality is different before and after the replacement. Even accounting for this artificial difference, though, the relative strength of activity at moulin A over moulin B is significantly higher starting on 31 July, which can also be partly verified from the original cross-correlation waveforms. While the cross-correlation peak corresponding to moulin A is observed at several station pairs (Figures 3g–3i), the peak for moulin B is observed only at the closest station pair (between stations 2 and 5; Figure 3i), which is why only moulin A is detected on 31 July, whereas moulin B is observed to be as active as moulin A or even more frequently observed before the precipitation on 29 July. This change may be a spurious change caused by geophone decoupling induced by precipitation (moulin A may still be observed because its relative cross-correlation amplitude is stronger than that of moulin B and is thus still seen after some decoupling). However, it is also possible that the change is due to spatial variability in moulin activity.

5. Discussion

5.1. Methodology

In this study, we primarily used passive seismic techniques, but other methods could have been useful. For example, satellites can directly image glacial hydrology features (e.g., Smith et al., 2015), but small supraglacial streams or small moulins can be difficult to distinguish from satellite images (e.g., King et al., 2016). We expect narrower streams to be more prevalent than wider ones, but the width frequency statistics in Greenland (Yang et al., 2016) has a peak at around 2 m, which implies that supraglacial streams as wide as 2 m are incompletely captured even from 0.5 m resolution images. On the other hand, the seismic-based technique has the potential to observe smaller moulins because we confidently capture 2 m wide moulins in this study, although smaller moulins have weaker and potentially higher frequency radiation that may be more difficult to capture using geophones. Satellite imaging would be appropriate to capture the distribution of large supraglacial rivers, but the seismic technique is more suitable for observing moulins associated with narrower streams in a relatively small area (e.g., on a specific mountain glacier). Passive seismic techniques also make continuous monitoring possible, which is challenging for satellite imaging. Another advantage of the seismic-based technique is the ability to directly distinguish the moulins that are actively supplying water to the subglacial system, which is difficult to tell from satellite images. For these reasons, passive seismic analysis is useful for glacier monitoring.

Using passive seismic analysis, Röösli et al. (2014) also located moulins as localized ambient noise sources. Their approach is different from ours in that they use decay of seismic amplitude over distances, rather than differential arrival times, to infer differential distance. While quality factors and wave velocities are unknowns in their method, we only require wave velocity, making our method more straightforward to implement. In addition, our method is insensitive to site response or the coupling

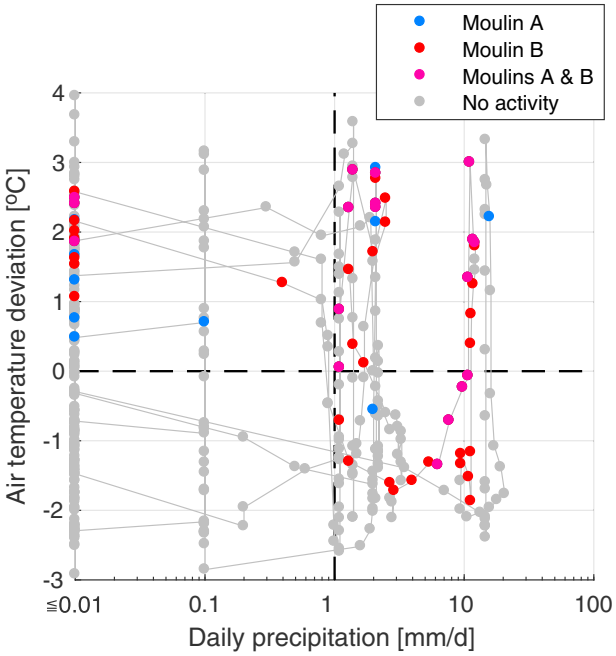

Figure 8. Crossplot of diurnal air temperature deviation and daily precipitation. The gray dots represent all hourly time periods in this analysis, and the blue and red dots represent detection of moulins A and B, respectively. the purple dots represent times when both moulins were active. The gray line represents the trace of temperature and precipitation. There are no events when the temperature is less than the daily mean temperature, and the daily mean precipitation is less than 1 mm/d. When the temperature is higher than the daily mean temperature and the daily mean precipitation is ≥1 mm/d, seismic activity is observed during 14 and 22 periods at moulins A and B, respectively, among 60 time periods. When the temperature is higher than its daily mean and the precipitation is <1 mm/d, we observe activity during 10 and 11 periods at moulins A and B, respectively, among 116 time periods. When the temperature is less than its daily mean and the precipitation is ≥1 mm/d, we observe activity during 5 and 15 periods at moulins A and B, respectively, among 98 time periods.

between instruments and ice, whereas that of Röösli et al. (2014) is critically dependent on knowing these properties, which are typically not well understood. Another advantage of using differential arrival time is that we can recognize multiple sources, while it is necessary to assume a single noise source to use the amplitude decay property. Röösli et al. (2014) were able to observe time-shifted seismograms between stations, which implies that the assumption of a single source was reasonable in their study. On the other hand, we cannot see explicit offsets in raw seismograms because of the existence of multiple sources that are simultaneously excited. Our method can distinguish multiple sources because cross correlation is a function of time and thus has vector information, whereas the method of Röösli et al. (2014) would not resolve them because only one scalar amplitude is considered at each station to estimate the decay of amplitudes. Walter et al. (2015) located the same moulin as Röösli et al. (2014) using differential arrival times of the same data in a manner similar to our method. They used cross-spectra in the frequency domain, which is the Fourier transform of the cross-correlation function in the time domain. They also tried to distinguish multiple sources by applying singular value decomposition (SVD). Our time domain analysis can also identify multiple sources as long as they are spatially separated, but we restrict the number of simultaneous sources to be two in this study because the third peak may be an artifact as described in the methodology section. The SVD of Walter et al. (2015) or other decompositions can potentially improve the detectability of smaller sources.

Another difference between our study and those of Röösli et al. (2014) and Walter et al. (2015) in Greenland is spatial coverage. In the present study, we resolve the locations of active moulins at high precision (50 m) from a relatively sparse geophone array (2 km station separation), compared to the 400 m separation in the previous studies in Greenland. This resolution indicates that it is feasible to capture moulin activity with an affordable number of geophone stations at each glacier. For example, tens of stations can cover a region that spans 4 km × 30 km, which is a reasonable number of stations for an observational campaign at an alpine glacier.

5.2. Glaciological Implications

We observe only surface waves, which do not have significant sensitivity to the noise distribution at depths greater than 100 m, so it is difficult to know whether these moulins extend all the way from the surface to the bed or if water in the moulin flows horizontally englacially, before dropping further to the bottom of the glacier at a later time. However, a lot of the energy in the flow would be dissipated where the falling water first impacts the ice or water surface in the moulin, so it is reasonable that strong noise sources are distributed near the surface, although there might be another strong source at depth that does not excite strong surface waves and is difficult to observe at remote geophone stations. Considering this seismic excitation mechanism at shallow depths, the seismic activity is a function of not only flow rate but also moulin geometry and water level in moulins. Taking those factors into consideration, we look at the temporal distribution of seismic activity at moulins.

One of our interesting observations is that moulin A became more active than moulin B after the precipitation event on 7/29, suggesting that either seismic coupling of the geophones changed or that the seismic radiation system of moulin A and/or moulin B changed after the rainfall. Specifically, it is possible that the geometry of the moulins changed after a significant amount of continuous flow into them. However, there are other possible causes for the differences before and after 7/29, including different distributions of precipitation and rerouting of supraglacial channels, about which we unfortunately have little information at this site. The

subglacial system also affects the seismic radiation efficiency (radiated seismic amplitude per unit flow rate) by changing the water level in moulins. For example, during the study period, a nearby lake probably started to drain (the lake started to drain at the very end of July or start of August and was fully drained by 8 August). The lake discharge likely increases the water pressure in the subglacial system and may lower the seismic radiation efficiency by increasing the water table level in moulins, but expected discharge near the lake is inconsistent with weaker radiation observed at moulin B that is more distant from the lake. Alternatively, it is possible that the subglacial drainage connected to moulin B did not efficiently drain for some reasons and increased water level in the moulin prevented strong seismic radiation.

Another interesting observation is that moulin activity is negatively correlated with temperature (Figure 7b) at timescales longer than a day. This anticorrelation is apparently inconsistent with the expectation of melt-controlled activity but can be explained simply because temperature anticorrelates with precipitation. If precipitation controls the activity at timescales longer than a day, we expect the apparent anticorrelation between temperature and activity, though this precipitation control may be localized (e.g., moulin B appears more affected than moulin A). Yet another possible nonphysical reason for the negative correlation is that surface melting may decouple the geophones from the ice and hence cause seismic signals to not be well recorded on warmer days. Alternatively, the correlation might be due to the physical relationship that higher temperatures might keep higher water levels in the moulins and cause seismic radiation to be less efficient. If changes in the coupling of geophones or in water level exist, observed seismic activity may not simply be related to flow rate at moulins and we may need to reexamine the effect of precipitation on seismic activity at longer timescales.

Water discharge is one of the variables we would like to measure but cannot yet directly estimate from seismic observations. Nonetheless, we expect the flow rate at our moulins to be roughly similar to that of the moulin at Sermeq Avannarleq studied by Röösli et al. (2014) for the following reasons: The horizontal size of moulins observed near cluster A in this study is ~2 m wide and is comparable to the moulin at Sermeq Avannarleq. Since the size of supraglacial streams (~2 m in width and decimeters in depth) and the slope of the ice surfaces (~2%) are similar, discharge through the moulins may be similar considering the empirical relationship between the geometry of rivers (including surface slope) and discharge (Williams, 1978).

Moulins are known to form from structural weaknesses such as crevasses (Holmlund, 1988), but their evolution is not yet well understood due to limited observations. Considering that there may be moulins at different stages of their life cycles (i.e., some young moulins that are newly developed from crevasses, some mature moulins that constantly drain water every summer, and some fossil moulins that have been shut down by creep closure and do not supply water to subglacial drainage any more), comparing different moulins is important for understanding the difference between young moulins and old moulins. Further, such studies on the statistical characteristics of moulin activity at other places ought to help us understand moulin evolution since our technique allows for capturing of drainage activity at multiple moulins simultaneously.

Finally, it is important to quantify the water flow rate for understanding the physics that causes moulins to be seismically active, but this is currently difficult for several reasons. First, the amplitude of the geophones used is not well calibrated, and the coupling between geophones and ice likely varied temporally because of melting. We could calibrate these amplitudes if we had enough local earthquakes, but we only have one M_w 6.0 event and its aftershocks at a distance of ~100 km from the observation site. Second, the relationship between water flow rate and generated seismic energy is dependent on models. For example, the seismic energy generated by turbulent flow is related to water flow rate in a complex manner (Gimbert, Tsai, & Lamb, 2014), and many other factors are also important, including the shape and roughness of the conduit. Alternatively, Röösli et al. (2016) proposed a model of a semiopen resonant vertical cylinder, but the effect of water flow rate on radiated energy was not studied well. The third difficulty of interpreting amplitude is due to complicated relationship between the cross-correlation amplitudes and the original seismogram amplitudes (Tsai, 2011). Cross-correlation amplitudes strongly depend on noise source distribution, and this unknown factor makes it difficult to utilize amplitude information in ambient noise interferometry. Although we have well-determined locations of localized noise sources within the array, we do not have good constraints on the noise source distribution outside the array. Once we overcome these difficulties, it may be possible to estimate flow rate only from the ambient seismic noise observations. Through such efforts, passive seismic studies at glaciers will contribute to a better and broader understanding of seismic noise generation processes.

6. Conclusions

Since moulins are a major source of subglacial water in areas of abundant surface melt, monitoring moulin activity is a practical way to monitor the subglacial hydrologic system, which has an important role in glacier dynamics. Although it is not straightforward to estimate subglacial conditions from water flow into moulins, the water supply into the subglacial system is fundamentally important and moulin activity is easier to monitor than subglacial drainage because of the localized nature of the source, its surface expression, and the signal strength due to the significant loss in gravitational potential energy involved in the descent of water into moulins. The microseismic noise generated at moulins has previously been reported at the Sermeq Avannarleq ablation zone near Jakobshavn Isbrae in Greenland (Röösli et al., 2014, 2016; Walter et al., 2015), while our study reports the first seismologically observed moulin activity in mountain glaciers.

Using a cross-correlation backprojection technique, we resolved seismic excitation from moulins. Diurnal activity is observed and suggests that temperature has a significant role in moulin activity as previously reported by McGrath et al. (2011). We find that precipitation correlates with seismic activity at longer timescales (primarily for only one of the two moulins observed), although its physical relationship needs further investigation. We suggest that water flow rate at some moulins may sometimes be dominated by precipitation rather than surface melt, though such a conclusion is unlikely to hold for a majority of moulins. Since weather conditions and supraglacial stream systems differ between glaciers, we cannot directly compare the moulins at different glaciers, but it is important to observe many moulins and study their statistics in the future. The cross-correlation backprojection technique is suitable for determining local sources within a seismic array, has a particularly strong advantage for measuring weak but continuous events, and is expected to be applied to localized sources of microseism tectonic tremors and volcanic tremors in the future.

Acknowledgments

We thank C. Zdanowicz and L. Copland for the meteorological data at the weather station at the confluence. We acknowledge the Natural Sciences and Engineering Research Council (NSERC) of Canada, the Canada Research Chairs Program, the California Institute of Technology, the University of British Columbia, and Simon Fraser University. We are grateful to the Polar Continental Shelf Program (PCSP) and Kluane Lake Research Station for logistical support. We are grateful to the Kluane First Nation, Parks Canada, and Yukon Territorial Government for permission to conduct field work. WorldView-1 imagery was obtained through the Polar Geospatial Center, University of Minnesota. This work was partially supported by the National Science Foundation grant EAR-1453263 and JSPS KAKENHI grant JP17H06605. Comments from two anonymous reviewers and the Associate Editor helped to improve the manuscript. Seismic data used in this paper are provided in the supporting information.

References

Amundson, J. M., Clinton, J. F., Fahnestock, M., Truffer, M., Lüthi, M. P., & Motyka, R. J. (2012). Observing calving-generated ocean waves with coastal broadband seismometers, Jakobshavn Isbræ, Greenland. *Annals of Glaciology*, *53*(60), 79–84. https://doi.org/10.3189/2012/AoG60A200

Andrews, L. C., Catania, G. A., Hoffman, M. J., Gulley, J. D., Lüthi, M. P., Ryser, C., … Neumann, T. A. (2014). Direct observations of evolving subglacial drainage beneath the Greenland ice sheet. *Nature*, *514*(7520), 80–83. https://doi.org/10.1038/nature13796

Bartholomaus, T. C., Amundson, J. M., Walter, J. I., O'Neel, S., West, M. E., & Larsen, C. F. (2015). Subglacial discharge at tidewater glaciers revealed by seismic tremor. *Geophysical Research Letters*, *42*(15), 6391–6398. https://doi.org/10.1002/2015GL064590

Bensen, G. D., Ritzwoller, M. H., Barmin, M. P., Levshin, A. L., Lin, F., Moschetti, M. P., … Yang, Y. (2007). Processing seismic ambient noise data to obtain reliable broad-band surface wave dispersion measurements. *Geophysical Journal International*, *169*(3), 1239–1260. https://doi.org/10.1111/j.1365-246X.2007.03374.x

Braithwaite, R. J. (1995). Positive degree-day factors for ablation on the Greenland ice sheet studied by energy-balance modeling. *Journal of Glaciology*, *41*(137), 153–160. https://doi.org/10.1017/S0022143000017846

Burkimsher, M. (1983). Investigations of glacier hydrological systems using dye tracer techniques: Observations at Pasterzengletscher, Austria. *Journal of Glaciology*, *29*(103), 403–416. https://doi.org/10.3198/1983JoG29-103-403-416

Burtin, A., Vergne, J., Rivera, L., & Dubernet, P. (2010). Location of river-induced seismic signal from noise correlation functions. *Geophysical Journal International*, *113*(B5), 1161–1173. https://doi.org/10.1029/2007JB005034

Carmichael, J. D., Joughin, I., Behn, M. D., Das, S., King, M. A., Stevens, L., & Lizarralde, D. (2015). Seismicity on the western Greenland Ice Sheet: Surface fracture in the vicinity of active moulins. *Journal of Geophysical Research: Earth Surface*, *120*, 1082–1106. https://doi.org/10.1002/2014JF003398

Carmichael, J. D., Pettit, E. C., Hoffman, M., Fountain, A., & Hallet, B. (2012). Seismic multiplet response triggered by melt at Blood Falls, Taylor Glacier, Antarctica. *Journal of Geophysical Research*, *117*(F3), F03004. https://doi.org/10.1029/2011JF002221

Chandler, D. M., Wadham, J. L., Lis, G. P., Cowton, T., Sole, A., Bartholomew, I., … Hubbard, A. (2013). Evolution of the subglacial drainage system beneath the Greenland ice sheet revealed by tracers. *Nature Geoscience*, *6*(3), 195–198. https://doi.org/10.1038/Ngeo1737

Chao, W. A., Wu, Y. M., Zhao, L., Tsai, V. C., & Chen, C. H. (2015). Seismologically determined bedload flux during the typhoon season. *Scientific Reports*, *5*(1), 8261. https://doi.org/10.1038/srep08261

Clarke, G. K. C. (2005). Subglacial processes. *Annual Review of Earth and Planetary Sciences*, *33*(1), 247–276. https://doi.org/10.1146/annurev.earth.33.092203.122621

Das, S. B., Joughin, I., Behn, M. D., Howat, I. M., King, M. A., Lizarralde, D., & Bhatia, M. P. (2008). Fracture propagation to the base of the Greenland Ice Sheet during supraglacial lake drainage. *Science*, *320*(5877), 778–781. https://doi.org/10.1126/science.1153360

Davis, J. L., de Juan, J., Nettles, M., Elosegui, P., & Andersen, M. L. (2014). Evidence for non-tidal diurnal velocity variations of Helheim Glacier, East Greenland. *Journal of Glaciology*, *60*(224), 1169–1180. https://doi.org/10.3189/2014JoG13J230

Denis, M., Guiraud, M., Konaté, M., & Buoncristiani, J.-F. (2010). Subglacial deformation and water-pressure cycles as a key for understanding ice stream dynamics: Evidence from the late Ordovician succession of the Djado Basin (Niger). *International Journal of Earth Sciences*, *99*(6), 1399–1425. https://doi.org/10.1007/s00531-009-0455-z

Doyle, S. H., Hubbard, A., Fitzpatrick, A. A. W., van As, D., Mikkelsen, A. B., Pettersson, R., & Hubbard, B. (2014). Persistent flow acceleration within the interior of the Greenland ice sheet. *Geophysical Research Letters*, *41*, 899–905. https://doi.org/10.1002/2013GL058933

Foo, S., & Kashyap, S. (2004). Cross-correlated back projection for UWB radar imaging, Antennas and Propagation Society International Symposium, 2004. *IEEE*, *2*, 1275–1278. https://doi.org/10.1109/APS.2004.1330417

Fountain, A. G., & Walder, J. S. (1998). Water flow through temperate glaciers. *Reviews of Geophysics*, *36*(3), 299–328. https://doi.org/10.1029/97RG03579

Gimbert, F., Tsai, V. C., Amundson, J. M., Bartholomaus, T. C., & Walter, J. I. (2016). Subseasonal changes observed in subglacial channel pressure, size, and sediment transport. *Geophysical Research Letters*, *43*(8), 3786–3794. https://doi.org/10.1002/2016GL068337

Gimbert, F., Tsai, V. C., & Lamb, M. P. (2014). A physical model for seismic noise generation by turbulent flow in rivers. *Journal of Geophysical Research: Earth Surface*, *119*, 2209–2238. https://doi.org/10.1002/2014JF003201

Heeszel, D. S., Walter, F., & Kilb, D. L. (2014). Humming glaciers. *Geology*, *42*(12), 1099–1102. https://doi.org/10.1130/G35994.1

Hock, R., & Hooke, R. L. (1993). Evolution of the internal drainage system in the lower part of the ablation area of Storglaciären, Sweden. *Geological Society of America Bulletin*, *105*(4), 537–546. https://doi.org/10.1130/0016-7606(1993)105%3C0537:EOTIDS%3E2.3.CO;2

Holmlund, P. (1988). Internal geometry and evolution of moulins, Storglaciären, Sweden. *Journal of Glaciology*, *34*(117), 242–248. https://doi.org/10.3198/1988JoG34-117-242-248

Hubbard, B. P., Sharp, M. J., Willis, I. C., Nielsen, M. K., & Smart, C. C. (1995). Borehole water-level variations and the structure of the subglacial hydrological system of Haut Glacier d'Arolla, Valais, Switzerland. *Journal of Glaciology*, *41*(139), 572–583. https://doi.org/10.3198/1995JoG41-139-572-583

Iken, A., & Bindschadler, R. A. (1986). Combined measurements of subglacial water pressure and surface velocity of Findelengletscher, Switzerland: Conclusions about drainage system and sliding mechanism. *Journal of Glaciology*, *32*(110), 101–119. https://doi.org/10.1017/S0022143000006936

Ishii, M., Shearer, P. M., Houston, H., & Vidale, J. E. (2005). Extent, duration and speed of the 2004 Sumatra-Andaman earthquake imaged by the Hi-Net array. *Nature*, *435*(7044), 933–936. https://doi.org/10.1038/nature03675

Johnson, P. G., & Kasper, J. N. (1992). The development of an ice-dammed lake: The contemporary and older sedimentary record. *Arctic and Alpine Research*, *24*(4), 304–313. https://doi.org/10.2307/1551285

Kapitsa, A. P., Ridley, J. K., de Q. Robin, G., Siegert, M. J., & Zotikov, I. A. (1996). A large deep freshwater lake beneath the ice of central. *East Antarctica*, *381*(6584), 684–686. https://doi.org/10.1038/381684a0

King, L., Hassan, M. A., Yang, K., & Flowers, G. (2016). Flow routing for delineating supraglacial meltwater channel networks. *Remote Sensing*, *8*(12), 988. https://doi.org/10.3390/rs8120988

Ma, Y., Clayton, R. W., Tsai, V. C., & Zhan, Z. (2013). Locating a scatterer in the active volcanic area of Southern Peru from ambient noise cross-correlation. *Geophysical Journal International*, *192*(3), 1332–1341. https://doi.org/10.1093/gji/ggs103

McGrath, D., Colgan, W., Steffen, K., Lauffenburger, P., & Balog, J. (2011). Assessing the summer water budget of a moulin basin in the Sermeq Avannarleq ablation region, Greenland Ice Sheet. *Journal of Glaciology*, *57*(205), 954–964. https://doi.org/10.3189/002214311798043735

Meng, L., Ampuero, J.-P., Sladen, A., & Rendon, H. (2012). High-resolution backprojection at regional distance: Application to the Haiti M7.0 earthquake and comparisons with finite source studies. *Journal of Geophysical Research*, *117*(B4), B04313. https://doi.org/10.1029/2011JB008702

Oswald, G. K. A., & de Q. Robin, G. (1973). Lakes beneath the Antarctic ice sheet. *Nature*, *245*(5423), 251–254. https://doi.org/10.1038/245251a0

Rial, J. A., Tang, C., & Steffen, K. (2009). Glacial rumblings from Jakobshavn ice stream, Greenland. *Journal of Glaciology*, *55*(191), 389–399. https://doi.org/10.3189/002214309788816623

Ridley, J. K., Cudlip, W., & Laxon, S. W. (1993). Identification of subglacial lakes using ERS-1 radar altimeter. *Journal of Glaciology*, *39*(133), 625–634. https://doi.org/10.3198/1993JoG39-133-625-634

Röösli, C., Walter, F., Ampuero, J.-P., & Kissling, E. (2016). Seismic moulin tremor. *Journal of Geophysical Research: Solid Earth*, *121*, 5838–5858. https://doi.org/10.1002/2015JB012786

Röösli, C., Walter, F., Husen, S., Andrews, L. C., Lüthi, M. P., Catania, G. A., & Kissling, E. (2014). Sustained seismic tremors and icequakes detected in the ablation zone of the Greenland Ice Sheet. *Journal of Glaciology*, *60*(221), 563–575. https://doi.org/10.3189/2014JoG13J210

Röthlisberger, H. (1972). Water pressure in inter- and subglacial channels. *Journal of Glaciology*, *11*(62), 177–203. https://doi.org/10.1017/S0022143000022188

Schoof, C. (2010). Ice-sheet acceleration driven by melt supply variability. *Nature*, *468*(7325), 803–806. https://doi.org/10.1038/nature09618

Shapiro, N. M., Ritzwoller, M. H., & Bensen, G. D. (2006). Source location of the 26 sec microseism from cross-correlations of ambient seismic noise. *Geophysical Research Letters*, *33*(18), L18310. https://doi.org/10.1029/2006GL027010

Smith, L. C., Chu, V. W., Yang, K., Gleason, C. J., Pitcher, L. H., Rennermalm, A. K., … Balog, J. (2015). Efficient meltwater drainage through supraglacial streams and rivers on the southwest Greenland Ice Sheet. *Proceedings of the National Academy of Sciences of the United States of America*, *112*(4), 1001–1006. https://doi.org/10.1073/pnas.1413024112

Stehly, L., Campillo, M., & Shapiro, N. M. (2006). A study of the seismic noise from its long-range correlation properties. *Journal of Geophysical Research*, *111*, B10306(B10). https://doi.org/10.1029/2005JB004237

Sundal, A. V., Shepherd, A., Nienow, P., Hanna, E., Palmer, S., & Huybrechts, P. (2011). Melt-induced speed-up of Greenland ice sheet offset by efficient subglacial drainage. *Nature*, *469*(7331), 521–524. https://doi.org/10.1038/nature09740

Tsai, V. C. (2011). Understanding the amplitudes of noise correlation measurements. *Journal of Geophysical Research*, *116*(B9), B09311. https://doi.org/10.1029/2011JB008483

van de Wal, R. S. W., Boot, W., van den Broeke, M. R., Smeets, C. J. P. P., Reijmer, C. H., Donker, J. J. A., & Oerlemans, J. (2008). Large and rapid melt-induced velocity changes in the ablation zone of the Greenland Ice Sheet. *Science*, *321*(5885), 111–113. https://doi.org/10.1126/science.1158540

Waechter, A., Copland, L., & Herdes, E. (2015). Modern glacier velocities across the Icefield Ranges, St Elias Mountains, and variability at selected glaciers from 1959 to 2012. *Journal of Glaciology*, *61*(228), 624–634. https://doi.org/10.3189/2015JoG14J147

Walter, F., Clinton, J. F., Deichmann, N., Dreger, D. S., Minson, S. E., & Funk, M. (2009). Moment tensor inversions of icequakes on Gornergletscher, Switzerland. *Bulletin of the Seismological Society of America*, *99*(2A), 852–870. https://doi.org/10.1785/0120080110

Walter, F., Roux, P., Röösli, C., Lecointre, A., Kilb, D., & Roux, P. F. (2015). Using glacier seismicity for phase velocity measurements and Green's function retrieval. *Geophysical Journal International*, *201*(3), 1722–1737. https://doi.org/10.1093/gji/ggv069

Williams, G. P. (1978). Bank-full discharge of rivers. *Water Resources Research*, *14*(6), 1141–1154. https://doi.org/10.1029/WR014i006p01141

Winberry, J. P., Anandakrishnan, S., & Alley, R. B. (2009). Seismic observations of transient subglacial water-flow beneath MacAyeal Ice Stream, West Antarctica. *Geophysical Research Letters*, *36*, L11502(11). https://doi.org/10.1029/2009GL037730

Yang, K., Karlstrom, L., Smith, L. C., & Li, M. (2016). Automated high-resolution satellite image registration using supraglacial rivers on the Greenland Ice Sheet. *IEEE Journal of Selected Topics in Applied Earth Observations and Remote Sensing*, *10*(3), 845–856. https://doi.org/10.1109/JSTARS.2016.2617822

Zwally, H. J., Abdalati, W., Herring, T., Larson, K., Saba, J., & Steffen, K. (2002). Surface melt-induced acceleration of Greenland ice-sheet flow. *Science*, *297*(5579), 218–222. https://doi.org/10.1126/science.1072708